International Journal of Precision Engineering and Manufacturing (2021) 22:1365–1379
https://doi.org/10.1007/s12541-021-00551-9

Online ISSN 2005-4602
Print ISSN 2234-7593

REGULAR PAPER

Development of 3D Resonant Elliptical Vibration Transducer for Dual-Frequency Micro-Dimple Surface Texturing

Saood Ali[1] · Rendi Kurniawan[1] · Tae Jo Ko[1]

Received: 29 June 2020 / Revised: 30 May 2021 / Accepted: 31 May 2021 / Published online: 10 June 2021

Abstract
This paper proposes a dual-frequency surface texturing method that generates small, round, drop-shaped micro dimples on a cylindrical surface. To achieve this, two devices were developed: a 3D resonant elliptical vibration transducer and a non-resonant displacement amplifier. The 3D resonant elliptical vibration transducer operates at high frequency (≈18 kHz) and has three vibration modes: one longitudinal vibration mode and two bending vibration modes. The one-dimensional displacement amplifier operates at low frequency (≈155 Hz). Finite element analysis was used to develop 3D resonant elliptical vibration transducer. One dimensional displacement amplifier was designed on the basis of single parallel flexure hinge mechanism and its working principle was based on non-resonant transducer. The feasibility of the proposed method was examined by performing a surface texturing experiment on Al6061-T6 material specimen. The wettability of the micro-dimple structured surface was also examined by measuring the water contact angle.

Keywords 3D elliptical vibration transducer · Displacement amplifier · 3D elliptical locus · Micro-dimple · Dual-frequency surface texturing · Water-contact angle

1 Introduction

Surfaces with sophisticated micro/nano structures, have been assimilating the attention of researchers in the recent time greatly [1]. These structured surfaces illustrate several new and improved features compared to a smooth surface. The production and application of these structured surfaces have been appealing topics in research in the last few decades [2]. Some of the applications of structured surfaces include optical retroreflective and antireflective structures [3], reducing the friction between mating surfaces [4], and the creation of superhydrophobic or super hydrophilic surfaces [5].

The generation of micro/nano structured surfaces with accuracy and efficiency is a challenging task and requires sophisticated devices. Some of the typical methods used for generation of micro/nano structures are laser surface texturing (LST) [6], electrical discharge texturing (EDT) [7], abrasive-jet machining (AJM) [8], laser beam machining (LBM) [9], electrochemical machining (ECM) [10], lithography, etching, and deposition [11]. LST is the most commonly used technique to generate micro-structured surfaces. Laser is extremely flexible and fast and provide excellent control of the shape and dimension of the texture. However, due to high intensity of the laser beam, there is collateral damage to the surface in addition to the textured surface. The LST technique also requires relatively expensive equipment, a clean environment, and high processing time, which makes it unsuitable for mass production [6][12].

Micro machining is a well-suited method to produce textured surfaces at the mass scale [13]. Micro grinding and ultra-precision diamond cutting have been successfully used for producing textured surfaces. With micro grinding, it is not possible to produce micro-dimple structures because of the radius of the grinding wheel tip. In ultra-precision diamond cutting, the cost of a single-point diamond cutting tool is very high, which restricts the functionality for mass production process.

Vibration-assisted machining (VAM) processes have been successfully used to make structured surfaces [14]. In VAM processes, the cutting tool vibrates at a constant frequency and amplitude. Vibrations can be applied in one or two directions. Such machining methods are known as

✉ Tae Jo Ko
tjko@yu.ac.kr

[1] School of Mechanical Engineering, Yeungnam University, 214-1 Dae-dong, Gyeongsan-si, Gyeongbuk-do 712-749, South Korea

one-dimensional and two-dimensional VAM. The features of the generated texture can be controlled by adjusting the various parameters, such as the vibration frequency, amplitude, depth of cut, and the use of resonance or non-resonance conditions.

Inspired by the concept of VAM, Greco et al. built a micro-positioning stage to produce dimples on a cylindrical surface [14]. Kurniawan and Ko used a single parallel bridge type mechanism actuated by a piezoelectric actuator to produce textured surface in a turning system [12]. Gandhi et al. used a plunging and sliding type method to produce a textured surface in a turning system [15]. Guo and Ehmann developed a tertiary motion generator (TMG) in which the cutting tool vibrates along an elliptical path to produce a textured surface in a cylindrical turning operation. This process is known as elliptical vibration texturing (EVT) [5]. Kurniawan et al. developed a two-frequency elliptical vibration texturing (TFEVT) method in which a high-frequency (ultrasonic) TMG and a low-frequency displacement amplifier (LFDA) work simultaneously to create a textured surface [16].

There has been no publication on using a three-dimensional resonant-mode vibration transducer for the generation of a micro-dimple textured surface. In this study, a dual-frequency surface texturing is proposed using a new three-dimensional resonant mode high-frequency (15–20 kHz) vibration transducer to efficiently incorporate 3D elliptical vibration cutting into conventional texturing. For conventional texturing, a one-dimensional single parallel four-bar displacement amplifier was developed. The organization of the paper is follows: the development of the transducer is explained with a simulation and experimental analysis. The development of the low-frequency displacement amplifier is then discussed, followed by experimental results and the conclusion.

2 Dual-Frequency Surface Texturing

The present method proposes the incorporation of 3D ultrasonic elliptical vibration cutting (UEVC) and one-dimensional conventional texturing (CT) to produce a micro-dimple textured surface. In a conventional texturing method [14], a single-frequency sinusoidal motion is applied at the tool tip in the depth-of-cut direction. In UEVC, ultrasonic vibrations are applied in the depth-of-cut direction and the cutting direction or feed direction, which results in an elliptical trajectory of the tool tip.

The UEVC method is used for cutting hard materials (with an H_RC value greater than 39) [17] and has advantages of reduced cutting forces, better surface finish [18], and increased tool life [19]. In the present method, 3D UEVC was applied in three directions: the depth-of-cut, feed, and cutting directions. The 3D UEVC method was incorporated with a 1-D CT method.

to create micro-dimples. Figure 1a illustrates the principle of the proposed method, and Fig. 1b shows the tool tip motion during surface texturing operation. The relative motion of the tool tip during surface texturing operation can be expressed as:

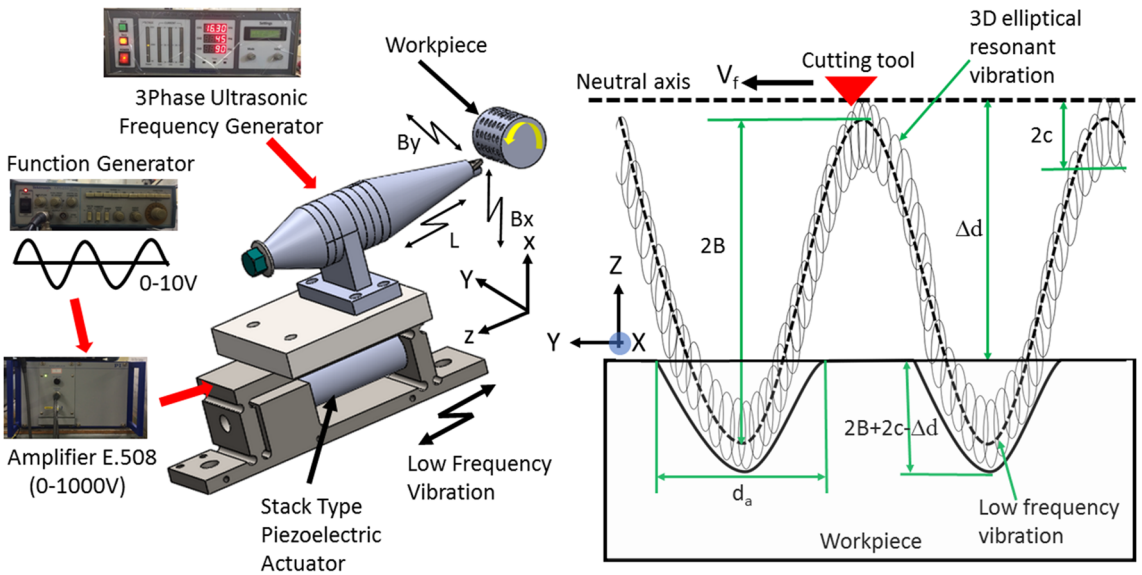

(a) Dual-frequency surface texturing principle **(b)** Tool-tip locus during texturing operation

Fig. 1 **a** Dual-frequency surface texturing principle, **b** Tool-tip locus during surface texturing operation

$$x(t) = a \cdot cos\left(2\pi f_h \cdot t + \varphi_{B_x}\right) \quad (1)$$

$$y(t) = b \cdot cos(2\pi f_h \cdot t + \varphi_{B_y}) + V_f \cdot t \quad (2)$$

$$z(t) = c \cdot cos\left(2\pi f_h \cdot t + \varphi_L\right) + B \cdot cos(2\pi f_l \cdot t) \quad (3)$$

$$2\pi f_h \cdot a > V_f \quad (4)$$

where $x(t)$, $y(t)$, and $z(t)$ are the positions of the tool tip in a three-dimensional Cartesian coordinate system, f_h is the high three-dimensional resonance frequency (≈20 kHz), f_l is the low one-dimensional frequency of a sinusoidal wave (100–200 Hz), Φ_{Bx}, Φ_{By}, and Φ_L are phase shifts, and V_f is the nominal relative cutting velocity.

The 3D elliptical locus of the tool tip has amplitudes of a, b, and c in the x, y, and z directions, respectively, while B is the amplitude of the low-frequency one-dimensional sinusoidal wave. The highlight of the UEVC method is the intermittent cutting [20], i.e. separation of the tool tip from the workpiece during the cutting and to achieve this, the maximum ultrasonic vibration velocity must be higher than the nominal cutting velocity V_f, as shown in Eq. 4. This condition remains true in the present method when the tool tip reaches the bottom of the micro-dimple.

3 Development of 3-Dimensional Resonant Vibration Transducer

The VAM system includes a vibration generator, vibration transducer, cutting tool, and vibration measuring devices (e.g., an optical sensor and oscilloscope) [12]. The vibration transducer is the heart of the system and is composed of lead zirconate titanate (PZT) ceramic (a full circle or half circle or combination of both depending upon the requirement), a horn for magnifying the vibration amplitude and efficiently transferring the vibration to the tool tip, a backmass for balancing the system, and a flange to fix the transducer. The design of the vibration transducer is the main problem in developing the VAM process. Piezoelectric transducers are preferred for VAM processes for numerous advantages such as high output amplitude, smaller size, and high energy conversion efficiency [21]. The number of transducers working in resonant mode has been developed previously but mainly for the purpose of elliptical vibration cutting [22–25].

3.1 Design Concept

In the present study the proposed 3D resonant vibration transducer is based on a sandwich structure and uses a single-node method to fix the transducer as shown in Fig. 2a and the physical property of each part is given in Table 1. The detailed description of the proposed device is shown in Fig. 2b. It consists of three sets of PZT ceramics (manufactured by SunnyTec company) in which one is full ring for longitudinal vibration, and the other two are half rings for X and Y bending vibrations. The induced electrical polarity of the three PZT ceramics sets is shown in Fig. 2c. The closest node point of all three vibrations was chosen as the mounting point for the flange. A preload bolt was used to clamp the device together since the proposed device is a type of bolt clamped Langevin transducer that uses the d_{33} working mode of PZT ceramics. The d_{33} working mode of PZT ceramics exhibit more output power and is more efficient [26].

The proposed transducer tends to work in the resonance mode, so the vibration modes of the tool tip should have same frequency in x-, y- and z- directions. This makes the process of

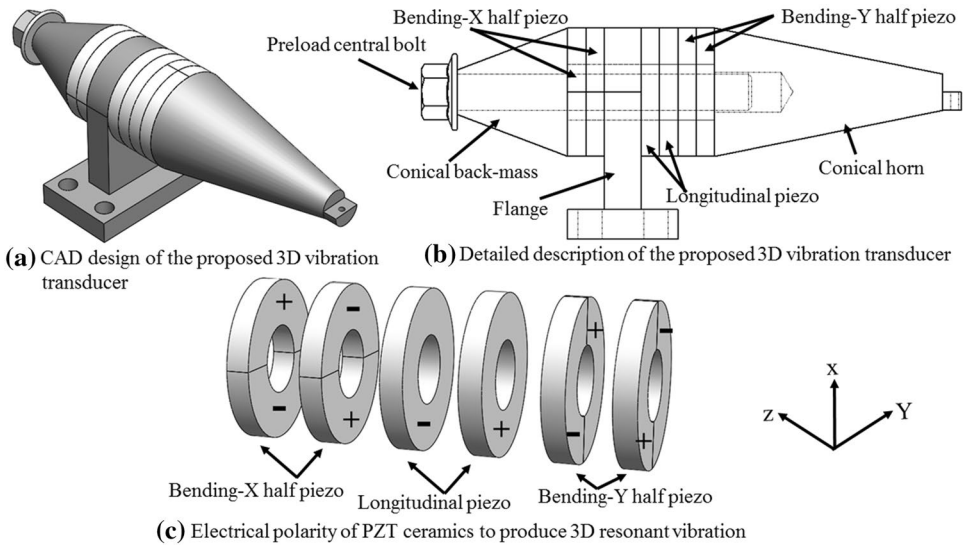

Fig. 2 **a** CAD design of the proposed 3D vibration transducer, **b** Detailed description of the proposed 3D vibration transducer, **c** Electrical polarity of PZT ceramics to produce 3D resonant vibration

Table 1 3D Vibration transducer component's material properties

S. No	Part	Material	Young's modulus (E) (GPa)	Mass Density (ρ) (kg/m^3)	Poisson ratio (μ)
1	Horn	Ti-6Al-4 V	105	4430	0.31
2	Back Mass	AISI 304	190	8000	0.28
3	Flange	AISI 1045	210	7800	0.28
4	Piezo	PZT-SS44	80	7700	0.33
5	Insulation	PTFE	0.5	2320	0.46
6	Preload Bolt	AISI 304	190	8000	0.28
7	Electrodes	Brass	100	8500	0.33

determining transducer dimensions extremely sensitive as the frequency should be same in all the three vibration directions to achieve the resonant condition. The initial dimension of the transducer was calculated based on the concept of a Langevin half-wavelength longitudinal vibration transducer as shown in Fig. 3a. The dimensions of the longitudinal vibration transducer were calculated by using Eqs. 5, 6, and 7 [27].

$$l_1 = \frac{c_1}{4f} = \frac{\lambda_1}{4}, c_1 = \sqrt{\frac{E_1}{\rho_1}} \tag{5}$$

$$tan\frac{4\pi f}{c_{01}}l_{01} \times tan\frac{4\pi f}{c_3}l_2 = \left(\frac{d_2}{d_1}\right)^2, c_{01} = \sqrt{\frac{E_{01}}{\rho_{01}}} \tag{6}$$

$$L_{3-1} = \frac{\lambda}{8} = \frac{c_3}{8f}, c_3 = \sqrt{\frac{E_3}{\rho_3}} \tag{7}$$

where c_1, c_{01}, and c_3 are the vibration velocity in the back-mass, PZT ceramic, and ultrasonic horn material, respectively. f is the vibration frequency, D_2 is the diameter of the PZT ceramics, and D_1 is the end-cap diameter of the ultrasonic horn. L_2 is the thickness of the flange, which is fixed at 10 mm to provide sufficient rigidity during the machining operation.

The longitudinal vibration device parameters were shown in Table 2. PZT bending ceramics with the same dimensions as the longitudinal PZT ceramics were inserted into the longitudinal device. The vibration frequency of the longitudinal mode and two bending vibrations were adjusted to be close to each other by adjusting the structure parameters.

3.2 Modal Analysis

To calculate the dimensions of 3D vibration transducer and coupled natural frequencies of three vibration modes, involving complex shape solids, method of sensitivity analysis was

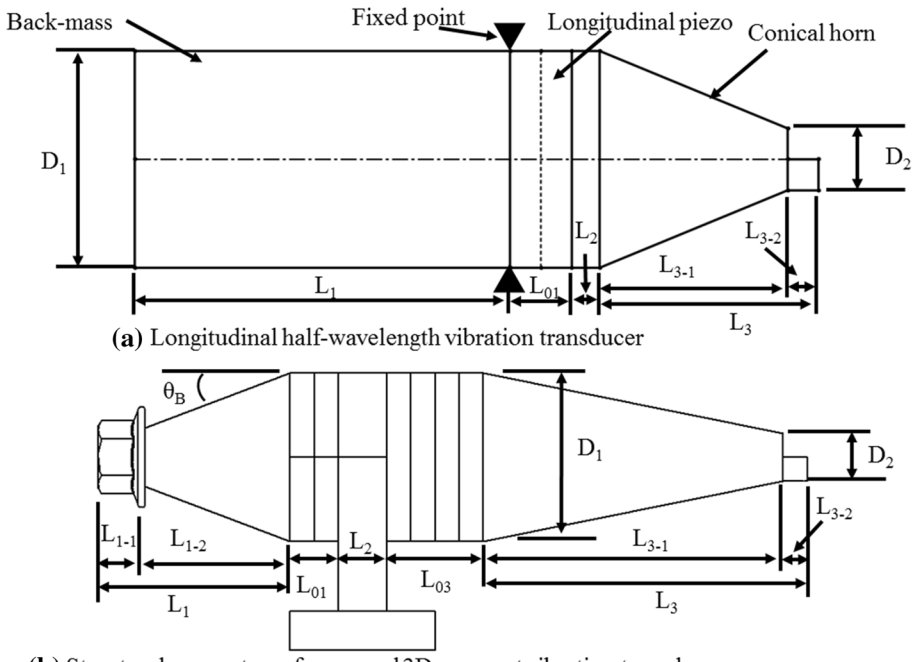

(a) Longitudinal half-wavelength vibration transducer

(b) Structural parameters of proposed 3D resonant vibration transducer

Fig. 3 **a** Longitudinal half-wavelength transducer, **b** structure parameters of proposed 3D resonant vibration transducer

Table 2 Half-wavelength longitudinal vibration device parameters

L_{01}	L_1	θ_B	L_3	$L_{3\text{-}1}$	$L_{3\text{-}2}$	L_2	D_2	D_1
10 mm	60.7 mm	0°	35.4 mm	30.4 mm	5 mm	4.5 mm	35 mm	10 mm

L_{01} = thickness of the Longitudinal PZT ceramics

Table 3 Final structural parameters of 3D vibration transducer

L_{01}	10 mm	$L_{3\text{-}1}$	62 mm
L_{03}	20 mm	$L_{3\text{-}2}$	5 mm
L_1	39.7 mm	L_2	10 mm
$L_{1\text{-}1}$	9.7 mm	D_2	35 mm
$L_{1\text{-}2}$	30 mm	D_1	10 mm
L_3	67 mm	θ_B	20.5 °

L_{01} = thickness of the bending-y PZT ceramics and brass electrodes

L_{02} = thickness of the longitudinal and bending-x PZT ceramics and brass electrodes

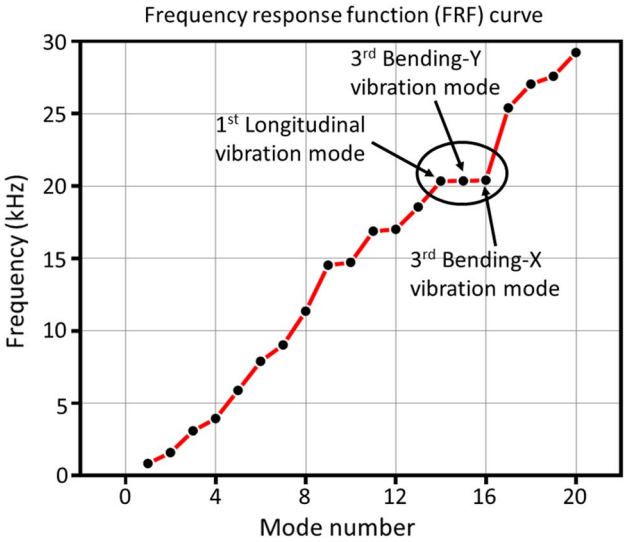

Fig. 4 Frequency versus mode shape analysis of 3D vibration transducer

adopted in the present study [28]. In the sensitivity analysis, one of the predicted dimensions was adjusted, and the output of the modal response was analyzed. The final dimensions of the transducer were determined by a modal simulation using finite element method (FEM) analysis in SolidWorks simulation software. Standard triangular meshing was used in the simulation. The element size was approximately 2.32 mm, and the total numbers of elements and nodes were 63,195 and 92,060, respectively. In FEM analysis, the tool insert, and insulation were neglected. The flange was placed between the longitudinal and bending-X ceramics. The natural frequencies of the longitudinal mode and two bending vibration modes were determined by adjusting the structure dimensions in such a way that the node point would always remain inside the flange.

Based on the modal analysis, the optimal design and structure parameters of the device were identified, as shown in Table 3. The frequency versus the mode shapes of the modal analysis is shown in Fig. 4. Mode shapes 14, 15, and 16 have the same frequency with no torsion vibration mode between them. After the modal analysis, the resonance frequency was found to be 20.30 kHz for longitudinal vibration, 20.33 kHz for bending-Y vibration, and 20.38 kHz for bending-X vibration. The three vibration mode shapes at resonant frequency are shown in Fig. 5. During the modal analysis, fixed boundary conditions were applied at the flange, as shown in Fig. 5.

3.3 Prototype 3D Vibration Transducer

To validate the design, a prototype 3D vibration transducer was developed based on the simulation results, as shown in Fig. 6. The whole transducer was held together by a preload bolt. Brass electrodes were placed between two PZT ceramics, and electric wire was attached to the electrodes to provide electric power. The bottom surface of the flange was screwed to a fixed support. Excitation signals were supplied to the PZT ceramics by a function generator (model NI6251, National Instruments). The generated sinusoidal signal was in the range of 0–10 V, and the output signal from the optical sensor amplifier was in the range of 0–5 V. The superposition of three resonant modes can be adjusted by changing the relative phase difference between them. Vibrations of the transducer were analyzed using an optical fiber sensor (Nanotex PM-15), which has a sensitivity, frequency range, working distance, and resolution of 12.6 µm/V, 100 Hz to 100 kHz, 77.6 µm, and 39.312 µm, respectively.

Sinusoidal sweep response analysis was done to determine the 3D resonant frequency of the developed transducer prototype. The frequency was swept continuously from 100 Hz to 25 kHz and travelled through the piezo amplifier (0–1000 V). The vibration amplitudes were measured using optical fiber sensors that were sequentially placed at the conical horn tip in the three mutually perpendicular directions as shown in Fig. 6. The response of the sinusoidal sweep test was analyzed by Fast Fourier Transformation (FFT) analysis as shown in Fig. 7. The first longitudinal, second bending-x, and fourth bending-y each had a resonance frequency of 20 kHz. This indicates that the developed prototype 3D

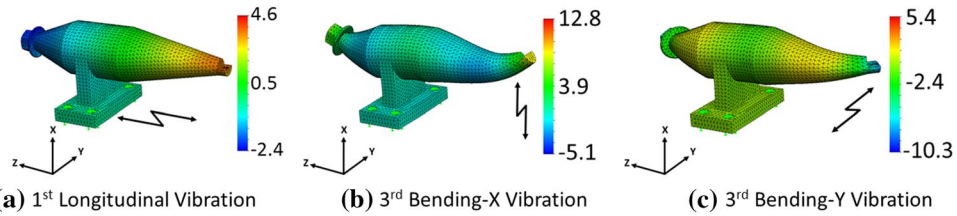

Fig. 5 Vibration mode shapes of 3D vibration transducer: **a** 1st longitudinal vibration, **b** 3rd Bending-X vibration, and **c** 3rd Bending-Y vibration

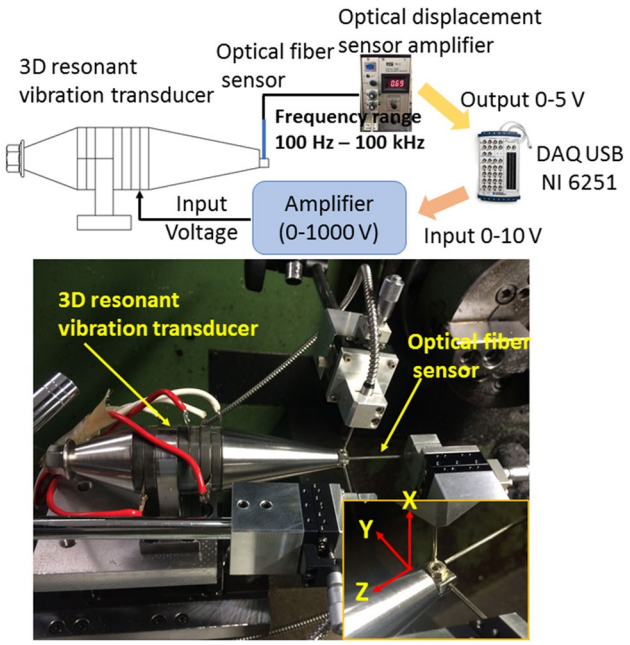

Fig. 6 Swept sine test setup to analyse the vibration frequency of the prototype 3D vibration transducer

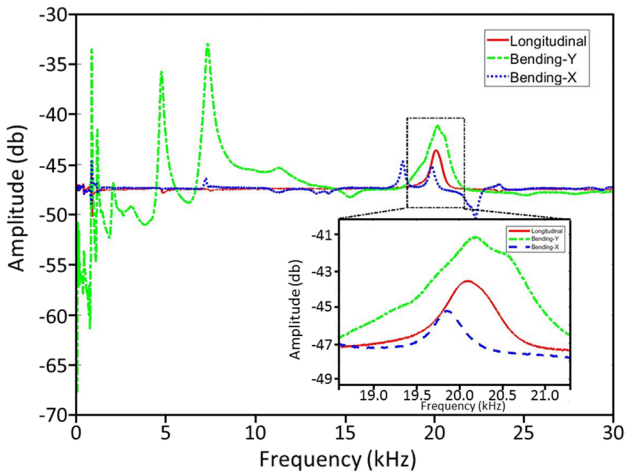

Fig. 7 FFT curve for sinusoidal sweep response analysis

vibration transducer was able to vibrate in three-dimensional space at resonant frequency. The frequency measurement results of simulation and FFT analysis were summarised in Table 4. The resonant frequencies identified from the experiment were always smaller than the FEM simulation result. This difference could result from imperfect fixed boundary conditions, differences between the ideal and actual material properties, meshing models, and manufacturing conditions.

Table 4 Summary of frequency tests

Vibration mode	Simulation Frequency (Hz)	Swept sine Frequency (Hz)
Longitudinal	20,304	20,100
Bending -Y	20,330	19,870
Bending-X	20,387	20,160

3.4 Analysis of Vibration Amplitude in Three-Dimensional Space

During the measurement of the displacement magnitude in three-dimensional Cartesian space, the 3D vibration transducer exhibits stable magnitude at a resonance frequency of 18 kHz instead of 20 kHz. The reason for this drop in resonant frequency is mainly the vibrations of the CNC lathe. Secondly, the 3D vibration transducer was also mounted on the CNC lathe through a low-frequency displacement amplifier and dynamometer, which also resulted in the loss of resonant frequency.

The transducer tip trajectory in three-dimensional Cartesian space with different phase differences between the three vibration modes (longitudinal (Φ_L), bending-y (Φ_{By}), and bending-x (Φ_{Bx})) is shown in Fig. 8. It has been observed that the magnitude of the 3D elliptical locus varies with the phase difference when the input voltage is kept constant, and it increases when the phase difference increases.

The effect of varying input voltage at the displacement amplitude of the three vibration modes with different phase difference is shown in Fig. 9. The displacement magnitude of the three vibration modes varies linearly with phase differences of 0°-45°-90° as compared to the other two cases of 0°-30°-60° and 0°-60°-120°. As a result, the 3D elliptical locus has a larger magnitude at phase differences of 0°-60°-120° than 0°-45°-90°, but the displacement variation with respect to the input voltage is more stable in the latter case. Therefore, the phase differences of 0°-45°-90° were chosen.

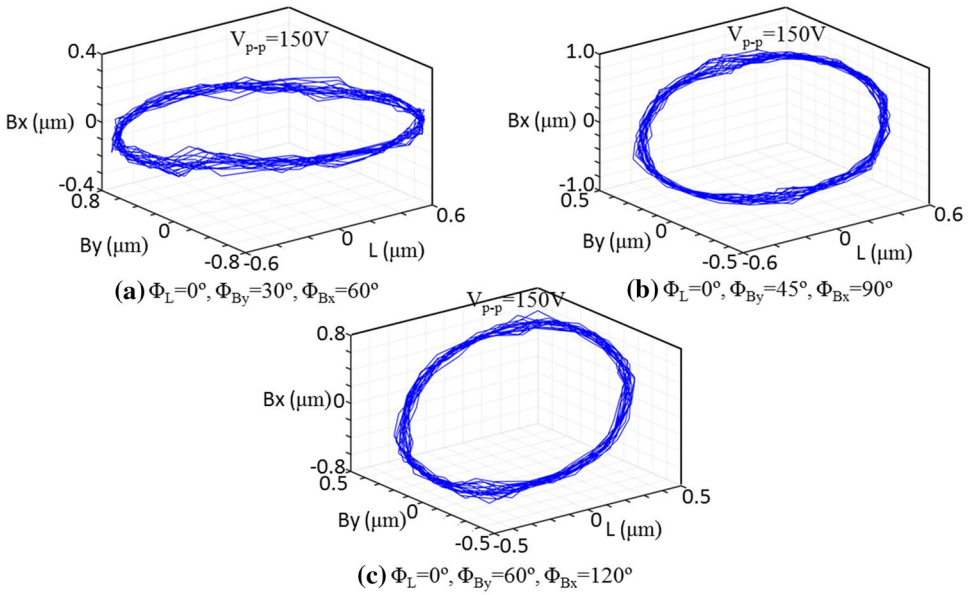

Fig. 8 Three-dimensional elliptical trajectory of vibration transducer tip in Cartesian space at resonance frequency of 18.0 kHz and input voltage of 150 V: **a** $\Phi_L = 0°$, $\Phi_{By} = 30°$ and $\Phi_{Bx} = 60°$, **b** $\Phi_L = 0°$, $\Phi_{By} = 45°$ and $\Phi_{Bx} = 90°$, and **c** $\Phi_L = 0°$, $\Phi_{By} = 60°$ and $\Phi_{Bx} = 120°$

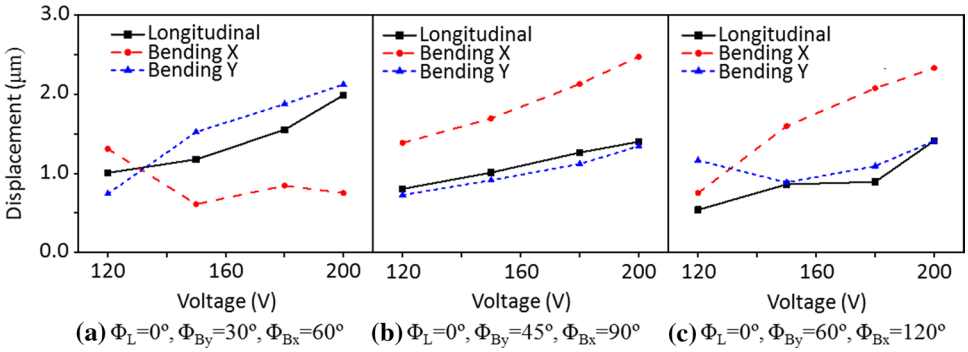

Fig. 9 Effect of varying input voltage on displacement amplitude

4 Low-Frequency Displacement Amplifier

The idea of two-frequency surface texturing was first introduced by Zhou et al. [29] to generate a freeform surface in diamond turning with a frequency of 100 Hz and spindle speed of 100 rpm. Zhou et al. [30] developed a double-frequency elliptical vibration cutting device that combines a fast tool servo and elliptical vibration cutting. Kurniawan et al. [16] developed a device for two-frequency elliptical vibration texturing. They used an ultrasonic elliptical motion transducer in conjunction with a low-frequency displacement amplifier to generate a textured surface. The idea of the present study was inspired by Kurniawan et al. [31] to use low-frequency displacement amplifier in conjunction with a high-frequency (18–22 kHz) vibration transducer to produce a micro-dimple textured surface.

The design of the low-frequency displacement amplifier is based on non-resonance frequency mode and has a much higher displacement amplitude than the locus amplitude of the 3D vibration transducer. The low frequency displacement amplifier is of double-spring single parallel flexure hinge type, and is equipped with a piezo stack actuator, as shown in Fig. 10. Its material properties and dimensions are given in Table 5. The displacement amplification ratio, r, was set to 5 to provide sufficient displacement to cut material. The flexure hinge mechanism eliminates friction. The piezo actuator is a stack-type (P-212.10 by Physik Instrumente). The maximum displacement of the piezo actuator under no external load is 15 μm, and it has a maximum force of 2000 N.

The concept of Lagrangian analysis [32] was used to compute the natural frequency f of the low-frequency displacement amplifier. The following assumptions are considered for this: (1) the rotation of the hinges is perfect, and (2) the displacement has a small magnitude under elastic deformation. Thus,

$$f = \frac{1}{2\pi}\sqrt{\frac{8K_r}{4I_A + m_B(l_1 - l_2)^2}} \tag{8}$$

where K_r is the rotational stiffness of the flexure mechanism, I_A is the moment of inertia of hinge A, and m_B is the mass of

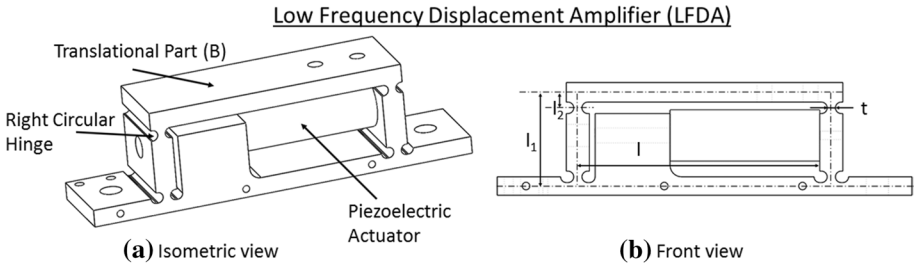

Fig. 10 Low-frequency displacement amplifier structure

Table 5 Material properties and dimensions of low-frequency displacement amplifier

S. No	Structural properties	
1	Material	AISI 4340 Steel
2	Young' Modulus (E)	205GPa
3	Shear Modulus (G)	80GPa
4	Density (ρ)	7850 kg/m^3
5	Width (b)	40 mm
6	Length (l)	110 mm
7	Hinge Radius (r)	2.5 mm
8	Minimum thickness of hinge (t)	3.55 mm
9	Distance between flexure hinges	l_1 = 36.75 mm l_2 = 6.75 mm

the translational part B, as shown in Fig. 11. K_r, I_A and m_B can be calculated according to He et al. [33].

The natural frequency of the low-frequency displacement amplifier mechanism was calculated as 1,572 Hz. Its displacement output without the preload of the piezoelectric actuator is calculated according to Zhu et al.[32]:

$$X = \frac{K_{pzt}}{K_{pzt} + K_{fh}} X_{nom} \tag{9}$$

where X_{nom} is the nominal displacement of the piezoelectric actuator, K_{pzt} is the nominal stiffness of the piezoelectric actuator, and K_{fh} is the stiffness of the mechanism. Based on Eq. 9, the displacement output is calculated as 8.66 µm.

The results of the swept-sine test of the low-frequency displacement amplifier are shown in Fig. 11. It was observed that the first natural frequency of the low-frequency displacement amplifier occurs at 1,374 Hz. However, the displacement magnitude of the low-frequency displacement amplifier decreases to a low value with the increase in frequency. The low-frequency displacement amplifier has a highest displacement magnitude occurred between 100 and 200 Hz.

For the generation of a micro-dimple textured surface, the low-frequency displacement amplifier should have higher displacement magnitude than the 3D vibration transducer. At a frequency of 155 Hz, the low-frequency displacement

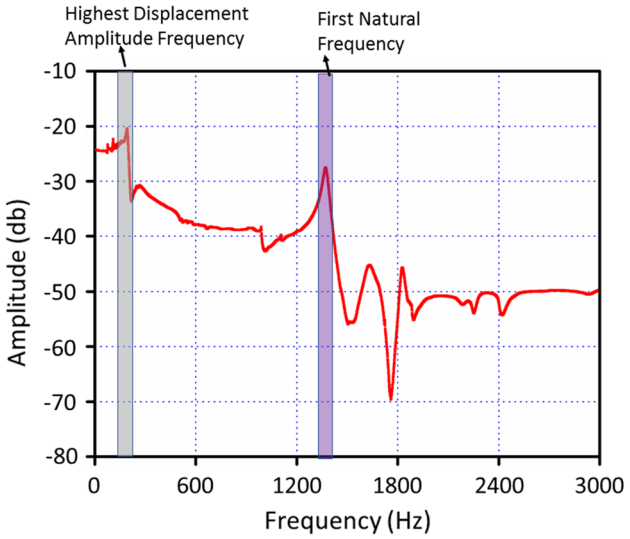

Fig. 11 Frequency response function of swept-sine test of low-frequency displacement amplifier

amplifier had a displacement magnitude of 22.5 µm, which is much higher than the displacement magnitude of the 3D vibration transducer. Also, the 3D resonant vibration transducer is mounted on LFDA, the operating frequency of the LFDA should below the first natural frequency so the whole system remains stable during the machining operation. Therefore, 155 Hz was selected as the working frequency of the low-frequency displacement amplifier.

5 Experimental Verification and Discussion

5.1 Experimental Set-up

The experimental setup for dual-frequency surface texturing is shown in Fig. 12. The workpiece is clamped in the spindle, and the 3D vibration transducer and low-frequency displacement amplifier are mounted on the slide of a CNC lathe. The micro-dimples are generated on a cylindrical specimen by controlling the rotational speed and the machining parameters.

Before the start of surface texturing, pre-machining was done to provide a smooth starting base and eliminate the mounting eccentricity of the workpiece. A PCD tool with a nose radius of 400 µm and a rake angle of 7° was used for the pre-machining. The machining parameters used for pre-machining were 0.01 mm/rev feed rate, 350 rpm spindle speed, and 10 µm depth of cut. After the pre-machining, the distance between the cutting tool and the premachined surface was adjusted to Δd (Fig. 1b). The experimental conditions are summarized in Table 6.

A 3-phase ultrasonic generator was used to excite the 3D elliptical vibration transducer at 150 V, 3D resonant frequency of 18.0 kHz, and phase differences of 0º-45º-90º between the longitudinal, bending-y, and bending-x vibration modes. The piezo actuator of LFDA mechanism was excited by a sinusoidal wave generated by a function generator (Tekntronix CFG 253) through a high voltage PZT-amplifier. The input voltage to the sinusoidal wave was 10 V with an amplitude of 22.5 µm at a frequency of 155 Hz.

Table 6 Experimental parameters

Workpiece Material	Al6061-T6
Diameter	28 mm
Tool Type	Poly Crystalline Diamond (PCD)
Low Vibration Frequency(f_l)	155 Hz
Low Vibration Frequency Amplitude	22.5 µm
3D Resonant Vibration Frequency(f_h)	18.0 kHz
Phase Shift (L-By-Bx)	0°-45°-90°
Spindle Speed	60 rpm
Feed rate	0.6 mm/rev
Δd	2.0 µm
3D elliptical locus amplitude	
Longitudinal	1.0 µm
Bending-X	1.6 µm
Bending-Y	0.8 µm

5.2 Experimental Results

During surface texturing, the low-frequency vibration is responsible for the creation of micro-dimple profile, while the high-frequency vibration is responsible for the intermittent contact between the tool and the machined surface. Six different textured surfaces were generated using six different vibration modes as summarized in Table 7.

The surface topography of the textured surfaces generated with different vibration modes are shown in Fig. 13. A white light non-contact 3D surface profilometer (NanoSystem NV-2000) is used to capture the textured surfaces. An isometric view of single micro-dimple and the micro-dimple profile along the feed direction has also analyzed as shown in Fig. 13. A 2D view of the micro-dimple textured surfaces were captured using an industrial microscope (NikonLV150) at 100 × and 200 × magnification as shown in Fig. 14.

The 3D-surface investigation of textured surfaces indicates that the micro-dimple shape is affected by the vibration modes applied. The addition of high frequency vibration modes makes the micro-dimple shape at the exit side of the cutting tool more circular instead of truncated cone type as shown in Fig. 14. The micro-dimples with 3D resonant vibration have the symmetrical circular ends.

An evaluation of cross-sectional view along the feed direction of the textured surfaces is presented in Fig. 13. The profile along the feed direction means that the 3D surface was cut by a plane along the feed direction. The micro-dimples feed direction profile shape follows the PCD cutting tool nose curvature, which has a nose radius of 400 µm. Absence of burrs along the micro-dimple profile shows the superior capability of the present method to create micro-dimple

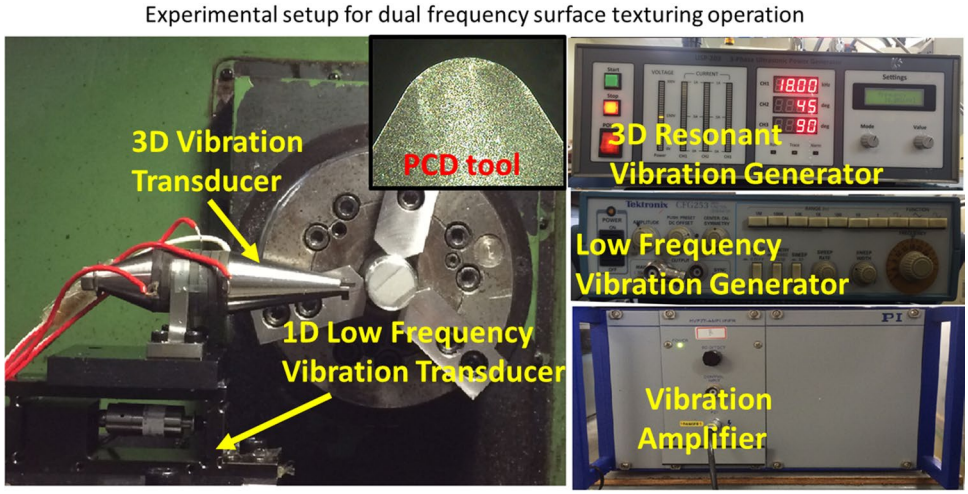

Fig. 12 Experimental setup for surface texturing operation

Table 7 Different vibration modes used for surface texturing

S. No	Vibration Mode	Designation
1	Low frequency vibration only	l
2	Low frequency + High frequency (Longitudinal) vibration	l + L
3	Low frequency + High frequency (Longitudinal + Bending-X) vibration	l + L + Bx
4	Low frequency + High frequency (Longitudinal + Bending-Y) vibration	l + L + By
5	Low frequency + High frequency (Bending- X + Bending-Y) vibration	l + Bx + By
6	Low frequency + High frequency (Longitudinal + Bending-X + Bending-Y) vibration	l + L + Bx + By

textured surfaces with minimum sides burrs. The micro-dimple geometric parameters are shown in Fig. 15. The addition of high-frequency vibration modes changes the surface of the micro-dimple from a planar to a wavy surface. The micro-scale high frequency vibration marks in the form of waves are observed inside the micro-dimple surface as demonstrated in Fig. 14.

5.3 Wettability Analysis

The wettability of the surface is one of the main characteristics that affect the lubrication characteristics. Firstly, Etsion highlights the effect of surface textures in improving the tribological performance of machine components by improving the lubrication properties of the textured surfaces [34]. At the same time, the effect of surface textures on the wettability have also been studied. Yan et al. studies the wettability of laser textured flat brass surfaces in different mediums to examine wettability transition [35]. Hosseinabadi et al. use ultrasonic vibration assisted face turning for improved wettability [36]. Lu et al. create micro dimples on surfaces using EVC to control the wettability [37].

The wettability characteristics indicate the lubrication performance of the sliding surfaces. As, higher the wettability, more is the lubricant flow over the surface and better is the lubrication.

The wettability was measured in terms of water contact angle (WCA) characterizing the hydrophilicity or hydrophobicity of the textured surface. In the present study, the effect of micro-dimples generated with different vibration modes on the surface wettability has been analyzed using sessile drop method [38]. The volume of all water droplet was kept at 10 µL and each experiment was repeated five times. The results were taken as the mean value to avoid the random errors. The shape of the typical water droplet along the feed direction has been shown in Fig. 16. The measured water contact angle values for different textured surfaces are shown in Fig. 17.

The textured surface with three-dimensional vibration modes shows the lowest water contact angle as compared to other surfaces. This indicates the addition of three-dimensional high frequency vibration modes to low frequency vibration results in the textured surface being hydrophilic as compared to textured surface with other vibration modes micro-dimples.

6 Conclusion

An efficient and flexible method to generate micro-dimple patterns on a cylindrical surface with controlled cross-section profiles is presented. A design of 3D resonant elliptical vibration transducer and a low frequency displacement amplifier mechanism has been presented. Subsequently, the frequency analysis has been performed analytically and experimentally to determine the working frequency for the dual-frequency surface texturing method of the system. The surface texturing operation has been performed on a cylindrical specimen successfully by integrating the developed system on a standard CNC lathe machine. The following conclusions can be drawn:

1. The dual frequency surface texturing method can be integrated on a standard turning lathe machine very efficiently to implement the surface texturing operation at industrial level.
2. Surface texture patterns in the form of micro-dimples are generated successfully and efficiently on a cylindrical surface using the dual-frequency surface texturing method.
3. The addition of high-frequency vibration modes to the low frequency vibration changes the micro-dimple profile with more symmetric micro-dimples are obtained with 3D resonant vibration modes.
4. The water droplet expands along the feed direction on micro-dimples with three-dimensional high frequency vibration modes, enhancing the hydrophilic performance of the textured surface and improve the wettability performance of the textured surface.

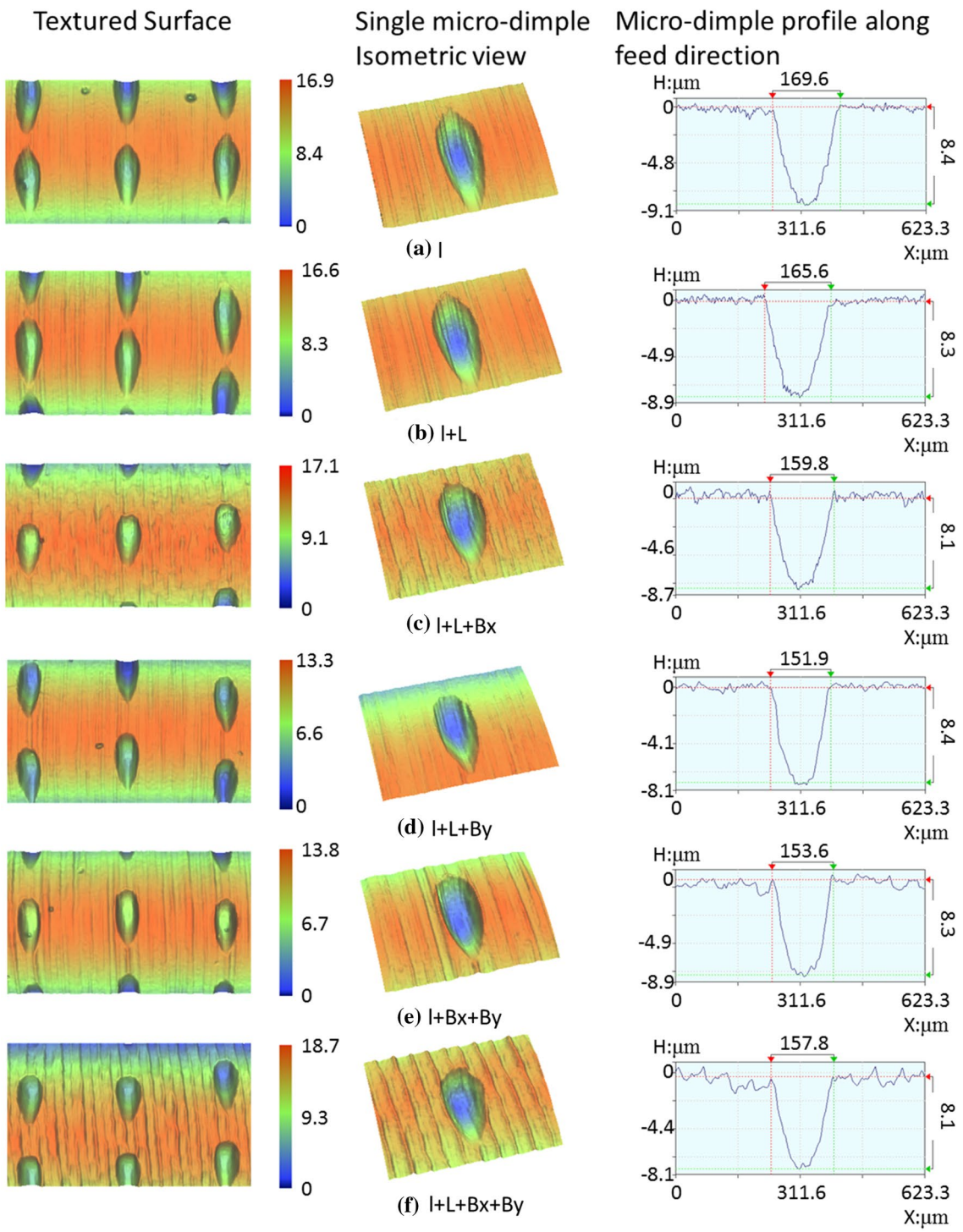

Fig. 13 3D surface morphology of the textured surface

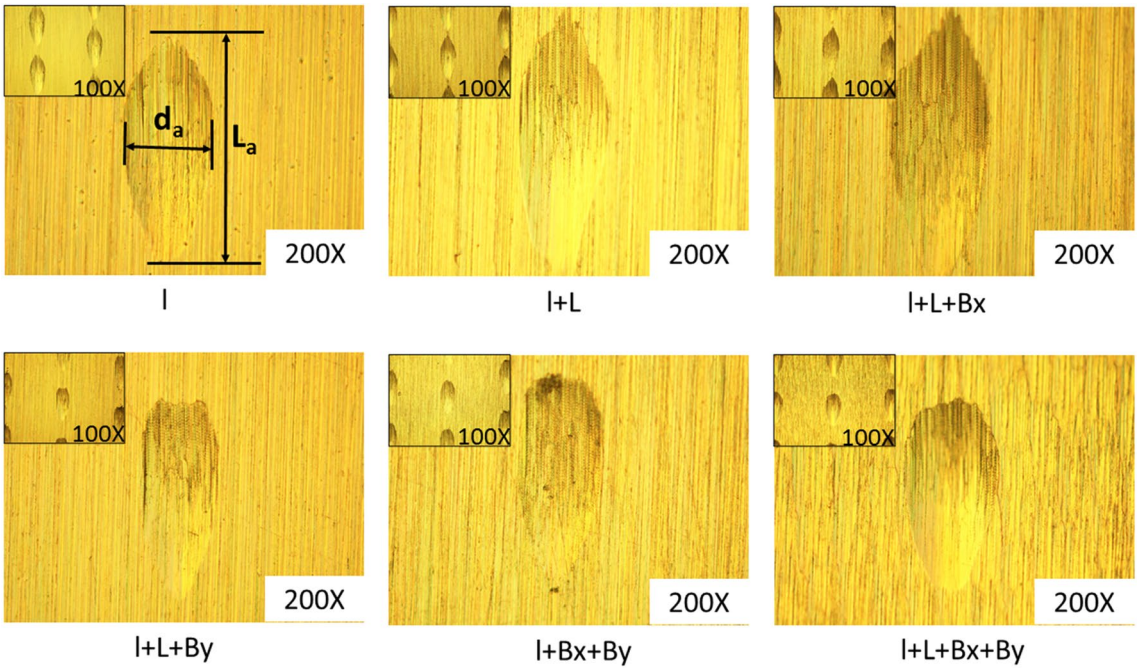

Fig. 14 2D view of the dimple-textured surface captured using Nikon LV150 industrial microscope

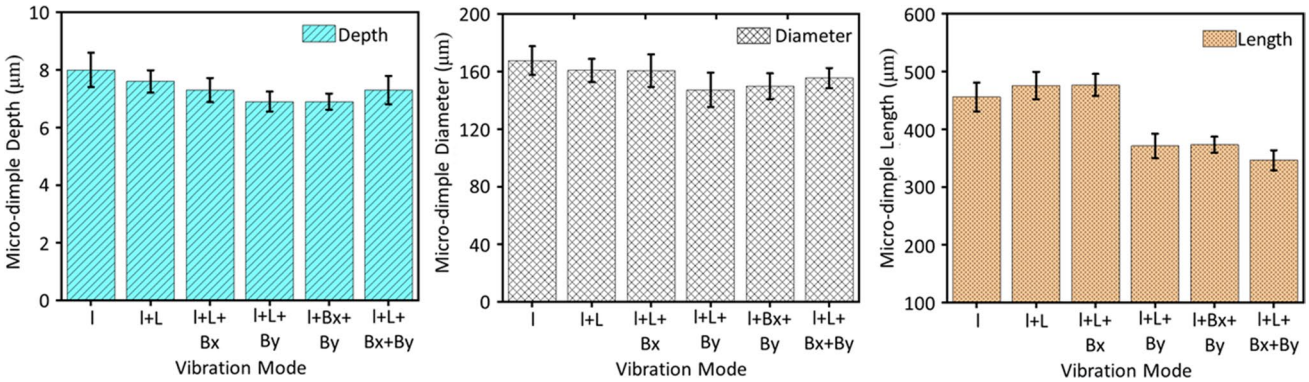

Fig. 15 Micro-dimple geometric parameters

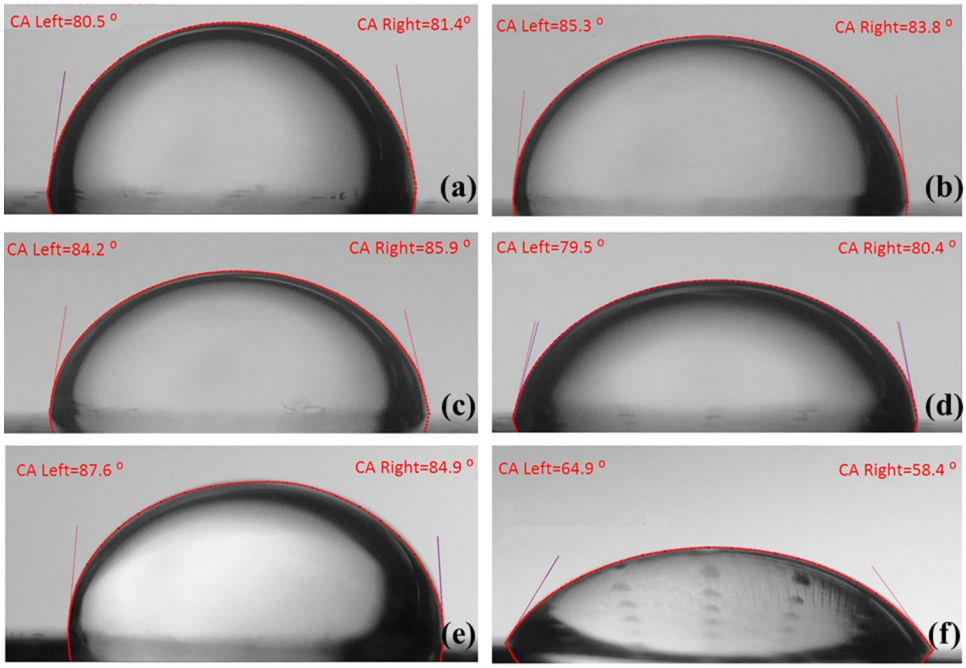

Fig. 16 Water contact angle measurement by sessile drop method for different vibration modes micro-dimples: **a** l, **b** l+L, **c** l+L+Bx, **d** l+L+By, **e** l+Bx+By, & **f** l+L+Bx+By

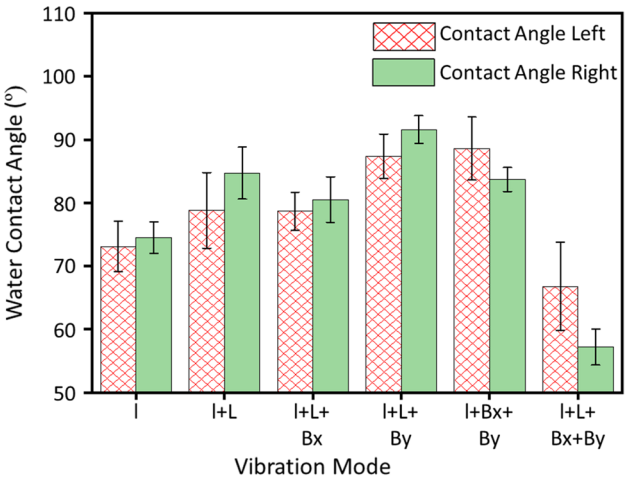

Fig. 17 Water contact angle analysis for different textured surfaces

Acknowledgements This research was supported by the Basic Science Research Program through the National Research Foundation of Korea (NRF) and funded by the Ministry of Science, ICT, and Future Planning (grant number NRF-2020 R1A2B5B02001755).

References

1. Xu, S., Kuriyagawa, T., Shimada, K., & Mizutani, M. (2017). Recent advances in ultrasonic-assisted machining for the fabrication of micro/nano-textured surfaces. *Frontiers of Mechanical Engineering, 12*, 33–45. https://doi.org/10.1007/s11465-017-0422-5
2. Zhang, J., Cui, T., Ge, C., Sui, Y., & Yang, H. (2016). Review of micro/nano machining by utilizing elliptical vibration cutting. *International Journal of Machine Tools and Manufacture, 106*, 109–126. https://doi.org/10.1016/j.ijmachtools.2016.04.008
3. Bruzzone, A. A. G., Costa, H. L., Lonardo, P. M., & Lucca, D. A. (2008). Advances in engineered surfaces for functional performance. *CIRP Annals-Manufacture Technology, 57*, 750–769. https://doi.org/10.1016/j.cirp.2008.09.003
4. Kurniawan, R., & Ko, T. J. (2015). Friction reduction on cylindrical surfaces by texturing with a piezoelectric actuated tool holder. *International Journal of Precision Engineering and Manufacturing, 16*, 861–868. https://doi.org/10.1007/s12541-015-0113-2
5. Guo, P., & Ehmann, K. F. (2011). Development of a new vibrator for elliptical vibration texturing, ASME 2011 Int. *Manufacture Science Engineering Conference MSEC, 2011*(1), 373–380. https://doi.org/10.1115/MSEC2011-50131
6. Vilhena, L. M., Sedlaček, M., Podgornik, B., Vižintin, J., Babnik, A., & Možina, J. (2009). Surface texturing by pulsed Nd:YAG laser. *Tribology International, 42*, 1496–1504. https://doi.org/10.1016/j.triboint.2009.06.003
7. Zhou, R., Cao, J., Wang, Q. J., Meng, F., Zimowski, K., & Xia, Z. C. (2011). Effect of EDT surface texturing on tribological behavior of aluminum sheet. *Journal of Materials Processing Technology, 211*, 1643–1649. https://doi.org/10.1016/j.jmatprotec.2011.05.004
8. Balasubramaniam, R., Krishnan, J., & Ramakrishnan, N. (2002). A study on the shape of the surface generated by abrasive jet machining. *Journal of Materials Processing Technology, 121*, 102–106. https://doi.org/10.1016/S0924-0136(01)01209-2
9. Wakuda, M., Yamauchi, Y., Kanzaki, S., & Yasuda, Y. (2003). Effect of surface texturing on friction reduction between ceramic and steel materials under lubricated sliding contact. *Wear, 254*, 356–363. https://doi.org/10.1016/S0043-1648(03)00004-8
10. Byun, J. W., Shin, H. S., Kwon, M. H., Kim, B. H., & Chu, C. N. (2010). Surface texturing by micro ECM for friction reduction. *International Journal of Precision Engineering and Manufacturing, 11*, 747–753. https://doi.org/10.1007/s12541-010-0088-y
11. Pettersson, U., & Jacobson, S. (2003). Influence of surface texture on boundary lubricated sliding contacts. *Tribology International, 36*, 857–864. https://doi.org/10.1016/S0301-679X(03)00104-X

12. Kurniawan, R., & Ko, T. J. (2013). A study of surface texturing using piezoelectric tool holder actuator on conventional CNC turning. *International Journal of Precision Engineering and Manufacturing, 14*, 199–206. https://doi.org/10.1007/s12541-013-0028-8
13. Dornfeld, D., Min, S., & Takeuchi, Y. (2006). Recent advances in mechanical micromachining. *CIRP Annal-Manufacturing Technology, 55*, 745–768. https://doi.org/10.1016/j.cirp.2006.10.006
14. Greco, A., Raphaelson, S., Ehmann, K., Wang, Q. J., & Lin, C. (2009). Surface Texturing of tribological interfaces using the vibromechanical texturing method. *Journal of Manufacturing Science and Engineering, 131*, 061005. https://doi.org/10.1115/1.4000418
15. Gandhi, R., Sebastian, D., Basu, S., Mann, J. B., Iglesias, P., & Saldana, C. (2016). Surfaces by vibration/modulation-assisted texturing for tribological applications. *International Journal of Advanced Manufacturing Technology, 85*, 909–920. https://doi.org/10.1007/s00170-015-7968-3
16. Kurniawan, R., Ko, T. J., Ping, L. C., Kumaran, S. T., Kiswanto, G., Guo, P., & Ehmann, K. F. (2017). Development of a two-frequency, elliptical-vibration texturing device for surface texturing. *Journal of Mechanical Science and Technology, 31*, 3465–3473. https://doi.org/10.1007/s12206-017-0635-x
17. Shamoto, E., & Moriwaki, T. (1999). Ultraprecision diamond cutting of hardened steel by applying elliptical vibration cutting. *CIRP Annals–Manufacturing and Technology, 48*, 441–444. https://doi.org/10.1016/S0007-8506(07)63222-3
18. Shamoto, E., Suzuki, N., Moriwaki, T., & Naoi, Y. (2002). Development of ultrasonic elliptical vibration controller for elliptical vibration cutting. *CIRP Annals–Manufacturing and Technology, 51*, 327–330. https://doi.org/10.1016/S0007-8506(07)61528-5
19. Nath, C., Rahman, M., & Neo, K. S. (2009). A study on ultrasonic elliptical vibration cutting of tungsten carbide. *Journal of Materials Processing Technology, 209*, 4459–4464. https://doi.org/10.1016/j.jmatprotec.2008.10.047
20. Shamoto, E., & Moriwaki, T. (1994). Study on elliptical vibration cutting. *CIRP Ann- Manufacture Technology, 43*, 35–38. https://doi.org/10.1016/S0007-8506(07)62158-1
21. Chen, T., Liu, S., Liu, W., & Wu, C. (2017). Study on a longitudinal-torsional ultrasonic vibration system with diagonal slits. *Advances in Mechanical Engineering, 9*, 1–10. https://doi.org/10.1177/1687814017706341
22. Tan, R., Zhao, X., Zou, X., & Sun, T. (2018). A novel ultrasonic elliptical vibration cutting device based on a sandwiched and symmetrical structure. *International Journal of Advanced Manufacturing Technology, 97*, 1397–1406. https://doi.org/10.1007/s00170-018-2015-9
23. Guo, P., & Ehmann, K. F. (2013). Development of a tertiary motion generator for elliptical vibration texturing. *Precision Engineering, 37*, 364–371. https://doi.org/10.1016/j.precisioneng.2012.10.005
24. Yang, Y., Gao, S., Chen, K., Pan, Y., & Guo, P. (2017). Vibration analysis and development of an ultrasonic elliptical vibration tool based on a portal frame structure. *Precision Engineering, 50*, 421–432. https://doi.org/10.1016/j.precisioneng.2017.06.016
25. Yin, Z., Fu, Y., Xu, J., Li, H., Cao, Z., & Chen, Y. (2017). A novel single driven ultrasonic elliptical vibration cutting device. *International Journal of Advanced Manufacturing Technology, 90*, 3289–3300. https://doi.org/10.1007/s00170-016-9641-x
26. Yang, X., Liu, Y., Chen, W., & Liu, J. (2013). Longitudinal and bending hybrid linear ultrasonic motor using bending PZT elements. *Ceramics International, 39*, S691–S694. https://doi.org/10.1016/j.ceramint.2012.10.163
27. Shuyu, L. (1995). Study on the multifrequency Langevin ultrasonic transducer. *Ultrasonics, 33*, 445–448. https://doi.org/10.1016/0041-624X(95)00051-4
28. Kurniawan, R., Ali, S., & Ko, T. J. (2018). Modal simulation analysis of novel 3D elliptical ultrasonic transducer. *IOP Conference Series Material Science and Engineering*. https://doi.org/10.1088/1757-899X/324/1/012063
29. Zhou Errata, X., Zuo, C., Liu, Q., & Lin, J. (2016). Surface generation of freeform surfaces in diamond turning by applying double-frequency elliptical vibration cutting. *International Journal of Machine Tools and Manufacture, 104*, 45–57. https://doi.org/10.1016/j.ijmachtools.2015.11.012
30. Zhou, X., Zuo, C., Liu, Q., Wang, R., & Lin, J. (2016). Development of a double-frequency elliptical vibration cutting apparatus for freeform surface diamond machining. *The International Journal of Advanced Manufacturing Technology*. https://doi.org/10.1007/s00170-016-8596-2
31. Kurniawan, R., Kiswanto, G., & Ko, T. J. (2017). Surface roughness of two-frequency elliptical vibration texturing (TFEVT) method for micro-dimple pattern process. *International Journal of Machine Tools and Manufacture, 116*, 77–95. https://doi.org/10.1016/j.ijmachtools.2016.12.011
32. Zhu, Z., Zhou, X., Liu, Q., & Zhao, S. (2011). Multi-objective optimum design of fast tool servo based on improved differential evolution algorithm. *Journal of Mechanical Science and Technology, 25*, 3141–3149. https://doi.org/10.1007/s12206-011-0824-y
33. He, Y., Zou, P., Zhu, Z., Le Zhu, W., Yang, X., Cao, J., & Ehmann, K. F. (2018). Design and application of a flexure-based oscillation mechanism for surface texturing. *Journal of Manufacturing Processes, 32*, 298–306. https://doi.org/10.1016/j.jmapro.2018.02.017
34. Etsion, I. (2004). Improving tribological performance of mechanical components by laser surface texturing. *Tribology Letters, 17*, 733–737. https://doi.org/10.1007/s11249-004-8081-1
35. Yan, H., Abdul Rashid, M. R. B., Khew, S. Y., Li, F., & Hong, M. (2018). Wettability transition of laser textured brass surfaces inside different mediums. *Applied Surface Science, 427*, 369–375. https://doi.org/10.1016/j.apsusc.2017.08.218
36. Hosseinabadi, H. N., Sajjady, S. A., & Amini, S. (2018). Creating micro textured surfaces for the improvement of surface wettability through ultrasonic vibration assisted turning. *International Journal of Advanced Manufacturing Technology, 96*, 2825–2839. https://doi.org/10.1007/s00170-018-1580-2
37. Lu, Y., Guo, P., Pei, P., & Ehmann, K. F. (2015). Experimental studies of wettability control on cylindrical surfaces by elliptical vibration texturing. *International Journal of Advanced Manufacturing Technology, 76*, 1807–1817. https://doi.org/10.1007/s00170-014-6384-4
38. Kurniawan, R., Ali, S., & Ko, T. J. (2020). Measurement of wettability on rhombohedral pattern fabricated by using 3D-UEVT. *Measurement, 160*, 107784. https://doi.org/10.1016/j.measurement.2020.107784

Mr. Saood Ali is doctoral candidate in Mechanical Engineering at Yeungnam University, South Korea. He received master's degree in material science engineering from Motilal Nehru National Institute of Technology Allahabad. His research interests are surface texturing, tribology, micro-dimple fabrication, and ultrasonic device development.

Mr. Rendi Kurniawan is currently assistant professor in Yeungnam University, South Korea. He received B.Eng degree from Universitas Indonesia, Indonesia. His M.S.Eng degree in mechanical engineering was acknowledged from Yeungnam University, South Korea. He received Ph.D degree in mechanical engineering from Yeungnam University. His research interests are surface texturing, tribology, friction reduction, micro-dimple fabrication, and elliptical vibration texturing.

Mr. Tae Jo Ko is a professor of mechanical engineering at Yeungnam University, South Korea. He received bachelor and master's degrees from Pusan National University, South Korea. He received Ph.D. in mechanical engineering from POSTECH, South Korea. His research interests include development of machine tools, micro-cutting process, non-traditional machining, surface texturing using grinding, bio-machining, hybrid EDM-milling process, textured surface on cutting tools and deburring process of CFRP composite.